Desalination and Water Treatment
www.deswater.com
doi: 10.1080/19443994.2013.874708

52 (2014) 1807–1819
February

Taylor & Francis
Taylor & Francis Group

Development and testing of a transparent membrane biofouling monitor

C. Dreszer[a,b], H.-C. Flemming[b], A.D. Wexler[a], A. Zwijnenburg[a], J.C. Kruithof[a], J.S. Vrouwenvelder[a,c,d,*]

[a]*Wetsus, Centre of Excellence for Sustainable Water Technology, Agora 1, P.O. box 1113, 8900 CC Leeuwarden, The Netherlands*
[b]*Biofilm Centre, University Duisburg-Essen, Universitätsstrasse 5, 45141 Essen, Germany*
[c]*Faculty of Applied Sciences, Department of Biotechnology, Delft University of Technology, Julianalaan 67, 2628 BC Delft, The Netherlands*
[d]*Water Desalination and Reuse Center, King Abdullah University of Science and Technology, Thuwal, Saudi Arabia*
Tel. +31 15 2784169; Fax: +31 15 2782355; email: j.s.vrouwenvelder@tudelft.nl

Received 28 September 2013; Accepted 17 November 2013

ABSTRACT

A modified version of the membrane fouling simulator (MFS) was developed for assessment of (i) hydraulic biofilm resistance, (ii) performance parameters feed-channel pressure drop and transmembrane pressure drop, and (iii) *in situ* spatial visual and optical observations of the biofilm in the transparent monitor, e.g. using optical coherence tomography. The flow channel height equals the feed spacer thickness enabling operation with and without feed spacer. The effective membrane surface area was enlarged from 80 to 200 cm^2 by increasing the monitor width compared to the standard MFS, resulting in larger biomass amounts for analysis. By use of a microfiltration membrane (pore size 0.05 μm) in the monitor salt concentration polarization is avoided, allowing operation at low pressures enabling accurate measurement of the intrinsic hydraulic biofilm resistance. Validation tests on e.g. hydrodynamic behavior, flow field distribution, and reproducibility showed that the small-sized monitor was a representative tool for membranes used in practice under the same operating conditions, such as spiral-wound nanofiltration and reverse osmosis membranes. Monitor studies with and without feed spacer use at a flux of 20 $L\,m^{-2}\,h^{-1}$ and a cross-flow velocity of 0.1 $m\,s^{-1}$ clearly showed the suitability of the monitor to determine hydraulic biofilm resistance and for controlled biofouling studies.

Keywords: Hydraulic biofilm permeability; Drinking water production; Treatment; Biofouling; Friction; UF; NF; RO; OCT; MFS; tMBM; Seawater desalination

1. Introduction

High quality water from water sources including seawater and sewage can be produced with membrane filtration processes like nanofiltration (NF) and reverse osmosis (RO). Because the global demand for clean fresh water is growing, the application of these membrane technologies has increased strongly [1].

One of the most serious problems in NF and RO applications is biofouling—biofilm formation causing unacceptable operational problems [1–7]. Biofilms may interfere with membrane performance in three ways: (i) increase of transmembrane pressure drop (TMP), (ii) increase of feed-channel (feed-concentrate)

*Corresponding author.

pressure drop (FCP), and (iii) decrease of salt rejection. According to manufacturer's specifications an operational problem of a membrane installation is defined when the transmembrane and/or feed-channel pressure drop (FCP) increase and/or salt rejection decrease exceed 15% of the start-up values [7–9]. When these parameters change by more than 15%, corrective actions must be taken and guarantees are restricted by the manufacturers of membrane elements. Biofouling, excessive growth of biomass, is an operationally defined problem affecting the performance of these membrane systems, influencing the amount and quality of the produced fresh water and costs.

In view of the relevance of biofouling, it is surprising how few data exist about the hydraulic resistance of biofilms that may affect the TMP and membrane passage. To investigate the effect of biofilm formation on a membrane system, it is essential to differentiate between the hydraulic resistance of the membrane and the fouling layer. Furthermore, intrinsic biofilms need to be obtained without disturbances by other fouling types, which is often not possible in NF and RO membrane systems. Therefore, a measurement of the clean water permeability of a fouled membrane module compared to a virgin module would not provide the pure biofilm resistance (since different fouling types and the module fouling distribution may play a role). Until now, there is no fouling simulation system available which allows the study of the intrinsic biofilm resistance without the influence of salt concentration polarization.

The objective of this study was to develop a transparent representative monitor with permeate production. The monitor should be suitable for assessment of (i) intrinsic hydraulic biofilm resistance, (ii) performance parameters: FCP and TMP, and (iii) *in situ* visual and optical spatial observations of the biofilm in the monitor. The boundary conditions for accurate and sensitive assessment of the intrinsic hydraulic biofilm resistance are exclusion of salt concentration polarization effects and operation at low pressures, resulting in the selection of a membrane with a pore size of 0.05 μm. The membrane fouling simulator (MFS), the monitor used in many research efforts [10–15], has shown to be representative for spiral-wound membrane modules used in practice. The MFS operated under cross-flow conditions without permeate production, gives identical results for fouling in a full-scale membrane module [16–18]. The original MFS was used as the prototype for the design of a monitor with permeate production to study the intrinsic hydraulic biofilm resistance.

2. Material and methods

2.1. Transparent membrane biofouling monitor (tMBM)

The tMBM is made of polymethylmethacrylate (PMMA). This transparent material offers the possibility to study biofilm growth *in situ*. The tMBM is suitable for cross-flow operation. Spatial dimensions and hydrodynamics are similar to spiral-wound NF and RO membrane elements. The external dimensions of the tMBM are $300 \times 170 \times 0.787$ mm, with 200 cm^2 of permeate producing membrane area. The feed-channel dimensions are $200 \times 100 \times 0.787$ mm (Fig. 1). The height of the feed-channel (0.787 mm) and the product spacer channel (0.25 mm) are based on reported data of spiral-wound membrane modules [19,20]. The height of the feed-channel is equivalent to the height of a 31 mil (787 μm) thick feed spacer enabling operating the system with or without feed spacer presence. The membrane is fixed in place by a frame on the edge of the feed-channel and is sealed by an O-ring. This construction prevents shifting of the membrane even without feed spacer presence. The large membrane area allows harvesting of a sufficient amount of biomass for analyses. The tMBM is equipped with one feed, one concentrate, and two permeate connections and can withstand pressures up to 5 bar. The pressure development over the feed-channel and the membrane can be measured via external connections at the feed, concentrate, and permeate inlets. During operation, the monitors are placed in opaque boxes to prevent growth of phototrophic organisms.

2.2. Membrane and spacer

The membranes used in this system were PES (polyethersulfone) microfiltration membranes (Nadir MP 005, Microdyn-Nadir GmbH Wiesbaden, Germany) with a pore size of 0.05 μm to enable operation at low pressure and prevent concentration polarization by salts. The 787 μm thick feed spacer consisted of polypropylene strings, arranged as a net structure with 90º angles and a porosity of about 0.85. This feed spacer is commonly used in spiral-wound NF and RO modules for water treatment in The Netherlands [21].

2.3. Setup configuration for operation of the transparent MBM

The test system [22] comprised four identical tMBMs which were installed as shown in Fig. 1. Feed

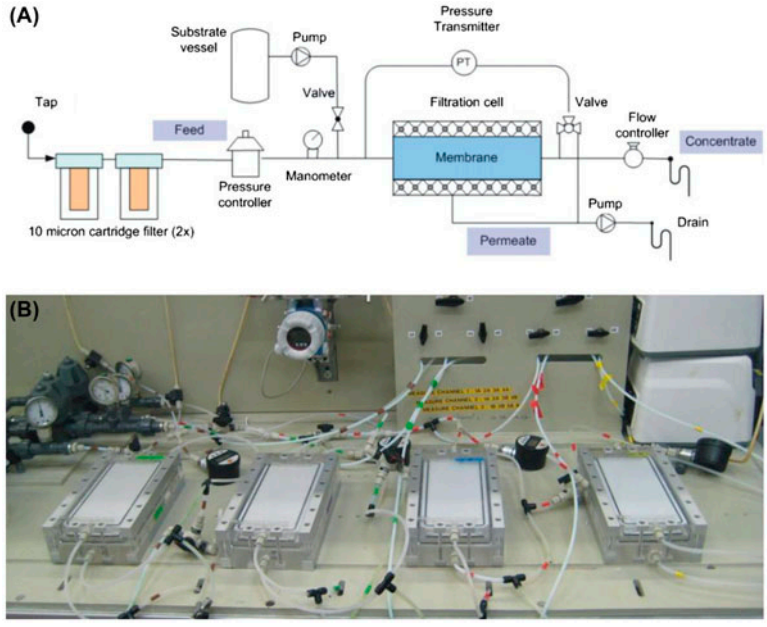

Fig. 1. (A) configuration of the filtration setup and (B) picture of four monitors in parallel.

water (see Section 2.4) was filtered through two 10 μm pore size cartridge filters and was kept constant at a temperature of 20°C. A pressure reducer (V782, Vink Kunststoffen B.V., Didam, The Netherlands) enabled a stable feed pressure of 1.7 bar for all experiments performed during the studies described in this paper. Before water entered the filtration cell, nutrients were added using a peristaltic pump (Masterflex L/S pumps, Cole-Palmer Instrument Company, Vernon Hills, Illinois, USA). The linear flow velocity of the feed water was monitored by a flow controller for each tMBM (8805/8905, Brooks Instrument, Hatfield, PA, USA) which was installed at the outlet of each monitor. The permeate rate was maintained by a peristaltic pump (Masterflex L/S pumps, Cole-Palmer Instrument Company, Vernon Hills, Illinois, USA). The fouling development was monitored by measuring the pressure drop over the feed-channel and over the membrane, using a differential pressure transmitter (Deltabar S PMD70, Endress + Hauser, Maulburg, Germany; [15]). The pressures were measured at the monitor inlet, permeate outlet, and concentrate outlet. Temperature, flow velocity, flux, FCP, TMP, and nutrient supply were measured twice a day.

2.4. Feed water for the transparent MBM experiments

Drinking water prepared from anaerobic groundwater (subsequently treated by aeration, rapid sand filtration, deacidification, softening, and rapid sand filtration at treatment plant Spannenburg in The Netherlands) is distributed without primary chemical disinfection and without a disinfectant residual. This drinking water was used as feed water source for the cross-flow filtration system experiments. The TCN in the feed water was 3×10^5 cells mL^{-1}. The number of colony forming units on R2A media [23] after 10 d incubation at 25°C was 2×10^3 CFU mL^{-1}. There are significantly more microbial cells in water than can be cultured on growth media [24,25].

As nutrients for the tMBM experiments, a solution of sodium acetate ($NaCH_3COO$), sodium nitrate ($NaNO_3$), and sodium di-hydrogen orthophosphate (NaH_2PO_4) in the mass ratio for C:N:P of 100:20:10, respectively, was employed at a final concentration of 1 mg L^{-1} of organic carbon. This nutrient composition has been used in several previous studies on biofilm formation and biofouling [10,12,15]. All chemicals were purchased in analytical grade from Boom B.V. (Meppel, The Netherlands). All chemicals were dissolved in milliQ water. The concentrated substrate solution (10 L) was dosed into the feed water prior to the filtration cell at a flow of 0.12 L h^{-1} using a peristaltic pump (Masterflex). The dosage of the nutrient solution was tested periodically by measuring the weight of the dosing container. To restrict bacterial growth in the substrate dosage bottle, the pH value was adjusted to 11 by NaOH addition. Fresh substrate solutions were prepared every 2 d. The chemical dosage flow rate (0.12 L h^{-1}) was low compared to the feed

water flow rate (28.2 L h^{-1}). So, the effect of the chemical dosage on the pH of the feed water was insignificant. The monitor was fed with 28.3 L per hour, requiring 28.3 mg acetate-C in the hourly dosed volume (0.12 L) of the concentrated acetate solution. The acetate-C stock solution concentration was 236 mg L^{-1} (28.3 mg/0.12 L), 236 times higher than the monitor feed water acetate-C concentration. The feed water before and after dosage of substrate and the concentrate had a pH value of 7.8. The nutrients were handled the same way as in previous research [10,12,15,22].

2.5. Biofilm characterization

The procedures for biofilm characterization were described in [22]. After the defined operation time, the transparent MBMs were opened and the biofilm was harvested with a cell scraper (TPP, St. Louis, MO, USA) and suspended in phosphate buffered saline; the solution was shaken for 30 min. Then, the biofilm sample was subjected to ultrasonic treatment (Bransonic, Berlin, Germany: model 5510E-DTH, output 135 W, 42 kHz), for 2 min. Afterwards, it was homogenized using an ultrasonic probe (Brandson Sonifier 250, G. Heinemann Ultraschall- und Labortechnik, Schwäbisch Gmünd, Germany) in pulsating mode (20% sonification per time-unit) for 10 pulses with an output of 45 W. The obtained biofilm suspension was used for total organic carbon (TOC) and total cell number (TCN) determination.

2.5.1. Resistance

Prior to biofilm analysis and during operation, the resistance (R) was determined on the basis of the following calculations:

$$R = \mathrm{TMP}/(\eta \times J)[\mathrm{m}^{-1}] \quad (1)$$

where TMP [Pa] is the transmembrane pressure, J [m^3 m^{-2} s^{-1}] is the permeate flux, and η [Pa s] is the dynamic viscosity of the water at a given temperature, in this study 20°C.

The TMP is the driving force for filtration. It is the average pressure difference between the feed and permeate:

$$\mathrm{TMP} = ((P_{\mathrm{inlet}} + P_{\mathrm{outlet}})/2) - P_{\mathrm{permeate}}\ [\mathrm{bar}] \quad (2)$$

The flux J of water passing a membrane is expressed as the amount of water V [L] flowing through a certain membrane area A [m^2] in time t [h]:

$$J = V/(A \times t)[\mathrm{Lm}^{-2}\mathrm{h}^{-1}] \quad (3)$$

The resistance in Eq. (1) is the sum of the membrane resistance and the resistance due to biofilm formation:

$$R_{\mathrm{total}} = R_{\mathrm{membrane}} + R_{\mathrm{biofilm}}\ [\mathrm{m}^{-1}] \quad (4)$$

The resistance measurement at $t = 0$ gives the virgin membrane resistance which is used to calculate the biofilm resistance:

$$R_{\mathrm{biofilm}} = R_{\mathrm{total}} - R_{\mathrm{membrane}} = R_{\mathrm{total}} - R_{\mathrm{total(t=0)}}\ [\mathrm{m}^{-1}] \quad (5)$$

2.5.2. TOC

To determine the TOC content of the biofilm (the sum of intra and extracellular organic carbon), an aliquot of the biofilm sample was placed in a TOC-free glass tube. The sample was treated with the ultrasonic probe (Brandson Sonifier 250, G. Heinemann Ultraschall- und Labortechnik, Schwäbisch Gmünd, Germany) in pulsating mode (20% sonication per time-unit) for 30 pulses with an output of 45 W. During the ultrasonic treatment, the sample was kept on ice for sample temperature control. The TOC was measured with a Shimadzu TOC analyzer (Shimadzu Scientific instruments, Kyoto, Japan).

2.5.3. TCN

A Neubauer Improved Counting Chamber was used for TCN determination of the biofilm sample. Bacterial cells were counted at 400× magnification with phase contrast using a Leica microscope (DM750, Leica, Wetzlar, Germany). Two times 5 squares were counted and the average value for 5 squares was taken for the calculation of the TCN by the following equation:

$$\mathrm{TCN} = \text{counted bacterial cells}/(\text{counted area } [\mathrm{mm}^2] \times \text{chamber depth } [\mathrm{mm}] \times \text{dilution})\ [\mathrm{cells}/\mu\mathrm{L}] \quad (6)$$

2.5.4. Scanning electron microscopy (SEM)

Pieces of membrane (~1 cm^2) were used for SEM of the biofilms. The samples were fixed in 3% glutaraldehyde (Sigma–Aldrich, Steinheim, Germany) at 4°C for 24 h, then washed twice in phosphate buffered saline and dehydrated in increasing concentrations of

Table 1
Schematic setup of studies

Studies[a]	Feed spacer presence	Permeate production	Cross-flow velocity (m s^{-1})	Substrate dosage (1 mg/L acetate C)	Section
Validation studies					3.1
Hydraulic characterization of monitor	yes	no	0–0.37	no	3.1.1
Flow field distribution	yes	no	0.1	no	3.1.2
Microfiltration use: internal fouling	no	yes	0.1	yes	3.1.3
Reproducibility	no/yes	yes	0.1	yes/no	3.1.4
Visual and optical observations	no	yes	0.1	yes/no	3.1.5
Application aspects of monitor					3.2
Biofilm characterization without feed spacer	no	yes	0.1	yes/no	3.2.1
Biofilm resistance with and without feed spacer	no/yes	yes	0.1	yes/no	3.2.2
FCP and biofilm resistance	yes	yes	0.1	yes/no	3.2.3

[a]All studies were carried out with 0.05 μm pore size membranes. The feed spacer was a 31 mil (787 μm) thick spacer as applied in practice. All studies with permeate production were performed at 20 L $m^{-2} h^{-1}$, except the reproducibility test (100 and 20 L $m^{-2} h^{-1}$). Nutrient dosage comprised 1 mg L^{-1} acetate C in the feed water.

ethanol (30, 50, 70, 90% for 20 min each; 96% for 30 min, twice). Finally, the samples were air dried in a drying chamber (45 °C, 30–60 min) and stored in a desiccator until microscopic investigation. To obtain the cross-section images, the pretreated membrane samples were placed in liquid nitrogen for shock freezing. At such low temperatures, the polymeric membrane and the organic biofilm became brittle. By breaking the frozen samples, sharp cross-sections without artifacts were obtained. The samples were sputtered with gold (Jeol JFC-1200 Fine Coater, Tokyo, Japan). SEM was performed with a JEOL JSM 6480 LV microscope (JEOL Technics Ltd., Tokyo, Japan) in high vacuum mode (emission electrons detection, acceleration voltage 6–10 kV, operating distance 10 mm).

2.5.5. Optical coherence tomography (OCT)

Imaging of the feed channel surface of the membrane was conducted *in situ* using a spectral domain optical coherence tomograph (Thorlabs Ganymede OCT System) fitted with a 5X telecentric scan lens (Thorlabs LSM03BB) which provides a maximum scan area of 100 mm^2. The OCT engine was configured to provide high resolution images with a sensitivity of 106 dB at 1.25 kHz A-scan rate. Volumetric images were created using the maximum intensity profile algorithm included in the instrument software (Thorlabs SD-OCT system software version 3.2.1) for a rectangular area 2 × 5 mm using from 200 B-scans and 500 A-scans of 619 pixels corresponding to a physical depth of 1.1 mm. The axial resolution for the instrument is below 5.8 μm and the lateral resolution is 8 μm.

2.6. Experiments and operational conditions

Temperature, flow velocity, feed pressure, flux, nutrient concentration, and operation time were constant throughout each set of experiments. FCP and TMP varied during operation time in response to biofilm formation. Flux and nutrient concentration differed from experiment to experiment to study the relation with biofilm permeability and operational parameters. Furthermore, the applicability of the tMBM as an essential research tool for biofilm studies was pursued. Table 1 gives an overview of the experiments.

3. Results

In this study, the tMBM was tested on suitability to study the hydraulic biofilm resistance (Section 3.1) and a number of monitor studies are presented to evaluate potential monitor applications (Section 3.2, Table 1).

3.1. Validation studies

3.1.1. Hydraulic characterization of the monitor

The relationship between linear flow velocity and FCP of the tMBM was calculated, using the methodology developed for spiral-wound membrane modules

as applied in practice [19]. Mathematically, the pressure drop is expressed by:

$$\Delta P = \lambda \times ((\rho \times v^2)/2) \times L/d_h \quad (7)$$

where λ is the friction coefficient, ρ the specific liquid density, v the linear velocity, L the length of the membrane or MBM, and d_h the hydraulic diameter. The friction coefficient is given by the correlation function [19]:

$$\lambda = 6.23 \times Re^{-0.3} \quad (8)$$

where Re is the Reynolds number. The measured relation between the linear flow velocity and pressure drop for the tMBM fitted very well with the calculated data using the formula for spiral-wound membrane elements (Fig. 2). Evidently, the tMBM had similar spatial dimensions (height of the feed spacer channel) as spiral-wound membrane elements applied in practice, resulting in an identical relation between linear flow velocity and pressure drop.

3.1.2. Flow field distribution

The flow field distribution in the tMBM was determined by injecting a pulse of a colored solution (blue ink) into the feed water. The front of the colored solution was equally distributed over the width of the tMBM (Fig. 3). The same flow regime was observed in the original MFS [16] and in spiral-wound membrane elements [26].

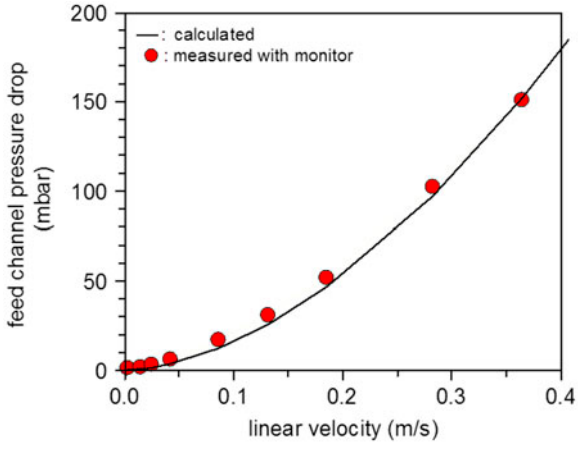

Fig. 2. Linear flow velocity (m s^{-1}) and FCP (mbar) in the tMBM containing a feed spacer. The dots represent measured data and the line represents calculated data using the formula for spiral-wound membrane elements of [19].

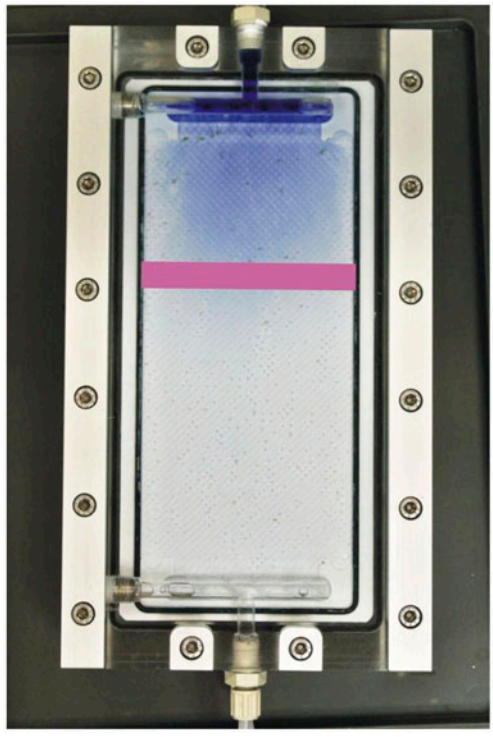

Fig. 3. The front of the blue dye spiked to the water equally distributed over the width during transport through the monitor, as illustrated with the purple bar.

3.1.3. Microfiltration membrane use: internal fouling

SEM observations. In order to operate the tMBM under low pressure conditions and to exclude salt concentration polarization effects, a 0.05 μm pore size membrane was selected. The hydraulic resistance of this membrane was expected to be significantly lower than the resistance of biofilms, enabling accurate and sensitive measurement of the hydraulic biofilm resistance. It is important to determine whether internal membrane fouling occurs, adding to the TMP. To evaluate this, a tMBM was operated at constant flux (20 L m^{-2} h^{-1}) and linear flow velocity (0.1 m s^{-1}), fed with tap water supplemented with a biodegradable nutrient (1 mg L^{-1} acetate C). During 4 d of operation accumulation of biomass on the membrane was observed visually through the transparent monitors. SEM examination (up to 10,000× magnification) of membrane samples taken from the tMBM, after that period of operation, showed that fouling accumulated only on the membrane surface and not in the membrane pores (Fig. 4). Clearly, the micro-organisms (≥~1 μm, Fig. 4) were retained by the membrane due to the pore size of the membrane (0.05 μm). No apparent fouling could be visually observed in the pores of the membrane [22].

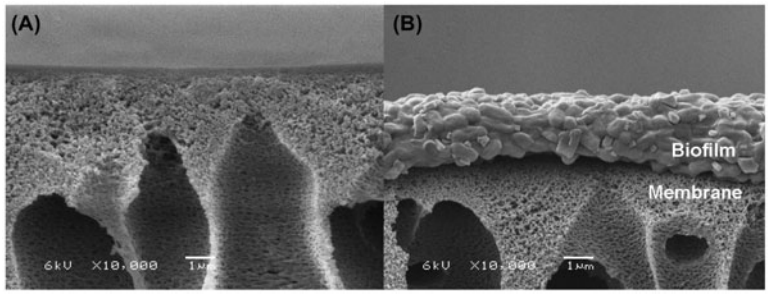

Fig. 4. Scanning electron micrograph of a membrane cross-section. (A) original membrane, (B) membrane with biofilm after 4 d of operation [22].

Resistance of virgin and mechanically cleaned membranes. In addition to the SEM analyses, the possibility of adsorption of macromolecules in the pores of the membrane affecting the resistance was determined by experiments performed under the same conditions (substrate, flux, and cross-flow velocity) as the SEM observations. The total resistance was determined before (virgin membrane), after fouling and after subsequent cleaning by removal of the biofilm. Experiments were performed in triplicate and biomass was removed by scraping. Scraping off the fouled membrane reduced the resistance to values similar to the virgin membrane resistance (Fig. 5). The scraped membrane had a resistance up to 5% higher than the virgin membrane probably caused by residual biofilm on the membrane surface. The effect of internal membrane fouling on the resistance is therefore negligible compared to the effect of fouling on the membrane surface (Fig. 5).

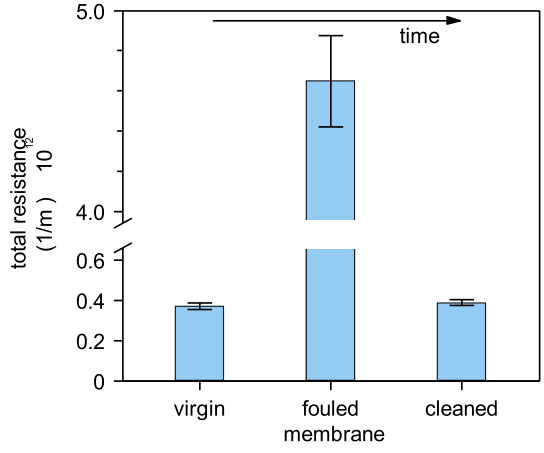

Fig. 5. Resistance prior to fouling (virgin membrane), after fouling, and after subsequent cleaning by scraping of the fouled membrane surface to remove the accumulated biofilm. A similar resistance of the virgin and cleaned membrane indicates that fouling predominantly occurred on the membrane surface [22].

3.1.4. Reproducibility

The reproducibility of the results obtained from the monitor experiments was examined. An experiment without feed spacer was repeated six times at the same flux ($100\,L\,m^{-2}\,h^{-1}$), linear flow velocity ($0.1\,m\,s^{-1}$), and substrate concentration ($1\,mg\,L^{-1}$ acetate C) for 4 d. The same development of total resistance and biomass accumulation (measured as TOC) was observed (Fig. 6). The average TOC concentration was $0.101 \pm 0.005\,mg\,cm^{-2}$, showing a 5% standard deviation.

Experiments conducted with feed spacer at a flux of $20\,L\,m^{-2}\,h^{-1}$ showed the same development of resistance and biomass (data not shown). Both reproducibility and comparability of results obtained with this test system and configuration were verified.

3.1.5. Visual and optical observations

The choice of PMMA as material for the tMBM enables visual and optical observations of biofilm development in time and spatial distribution over the membrane surface during tMBM operation (Fig. 7). To investigate the visual appearance of the biofilm, two tMBMs were operated in parallel for 4 d at a constant flux and cross-flow velocity without feed spacer. For one tMBM, the feed water was supplemented with additional nutrients ($1\,mg\,L^{-1}$ acetate C), while the other monitor had no nutrient dosage (blank).

With nutrient dosage a more rapid accumulation of material on the membrane was observed. The material seemed to be equally distributed over the membrane surface area by visual inspection during tMBM operation. The material accumulated gradually in time. A distinct difference in color was detected

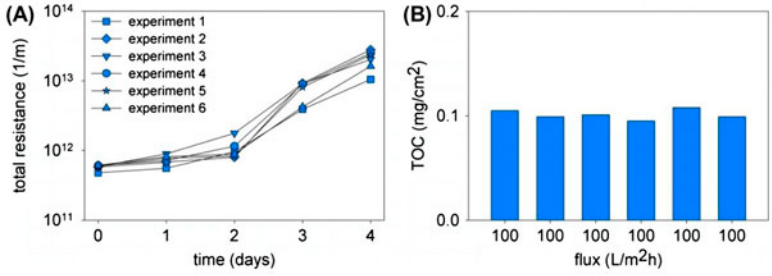

Fig. 6. Development of the total resistance for six experiments operated at a flux of 100 L $m^{-2} h^{-1}$ at a cross-flow velocity of 0.1 m s^{-1} with a substrate dosage of 1 mg L^{-1} acetate C in the feed water (A) and the amount of accumulated biomass at the end of the operational period (B).

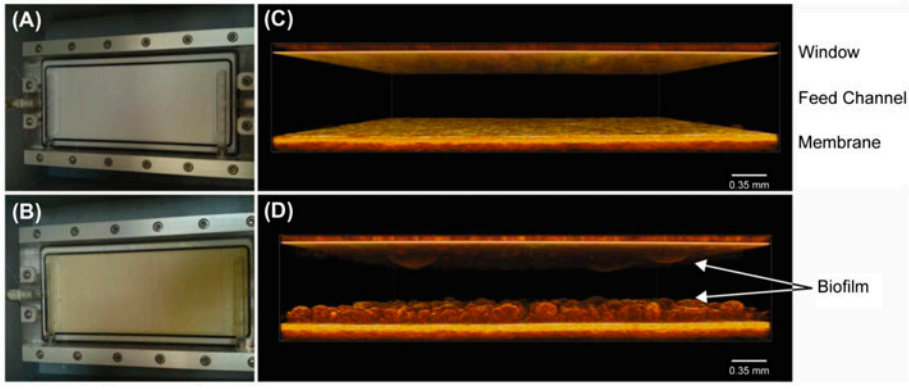

Fig. 7. Visual observations and OCT images for the feed channel in the tMBM after 4 d operation without ((A), (C)) and with dosage ((B), (D)) of a biodegradable substrate to the feed water.

between the tMBM with and without substrate dosage (Fig. 7). With nutrient dosage the accumulated material had a darker color. *In situ* OCT imaging confirmed biofilm formation throughout the feed-channel of the monitor supplied with substrate (Fig. 7(C) and (D)). The scanned rectangular area of 2 × 5 mm showed a heterogeneous biofilm structure on the membrane, varying in thickness from a few μm to ~200 μm. The structure of the biofilm growing on the window differed from the structure growing on the membrane. Biochemical analysis after 4 d tMBM operation confirmed that biomass had accumulated on the membrane with substrate dosage. The transparent MBM is suitable to study biofouling development using *in situ* non-destructive visual and optical observations.

3.2. Application aspects of monitor

Application aspects of the transparent MBM were tested in a series of experiments to evaluate the suitability of the monitor.

3.2.1. Biofilm characterization without feed spacer

The development of transmembrane resistance and biofilm amount was determined using tMBMs without feed spacer at a flux of 20 L $m^{-2} h^{-1}$. In a parallel study, four tMBMs were operated without nutrient dosage and four tMBMs with nutrients dosage (1 mg L^{-1} acetate C). After day 1, 2, 3, and 4 of operation, a tMBM with and a tMBM without nutrient dosage were opened for biomass quantification.

With nutrient supply, a strong increase of total resistance (Fig. 8(A)) and biomass amount (Fig. 8(B) and (C)) in time was found. After 4 d of operation, the total resistance was about 50 times higher than the intrinsic resistance of the 0.05 μm pore membrane (Fig. 8(A)). This difference in resistance enables distinguishing the resistance of the biofilm from that of the membrane. After 4 d of operation, the bacterial cell number and TOC concentration on the membrane were several log-units higher in the nutrient supplied system (Fig. 8(B) and (C)), indicating that biomass accumulated predominantly as a growing biofilm.

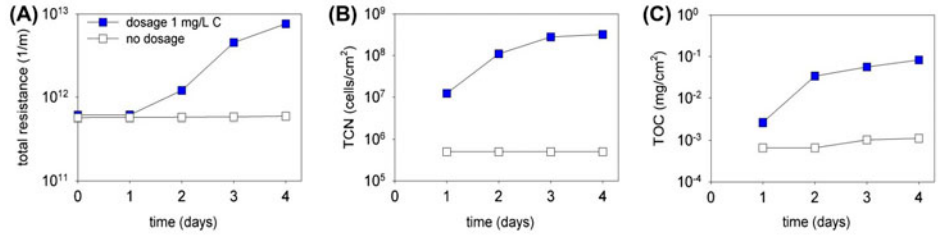

Fig. 8. Development of total resistance (A), TCN (total bacterial cell number: (B)) and TOC (total organic carbon: (C)) without feed spacer presence during 4 d of operation at a flux of 20 L $m^{-2} h^{-1}$ and cross-flow velocity of 0.1 m s^{-1} with and without nutrient dosage (1 mg L^{-1} acetate (C)). The increase in resistance is caused by the biofilm formation.

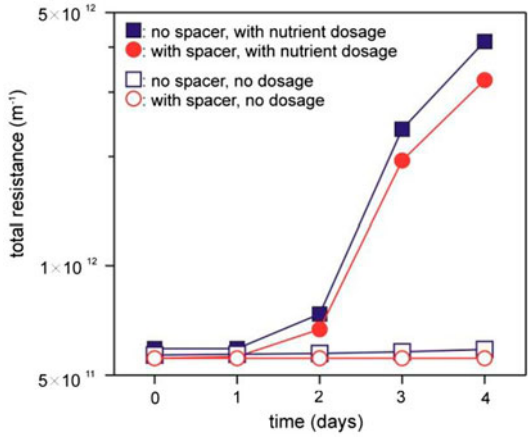

Fig. 9. Development of total resistance in monitors with and without feed spacer during 4 d at a flux of 20 L $m^{-2} h^{-1}$ and cross-flow velocity of 0.1 m s^{-1} with and without nutrient dosage (1 mg L^{-1} acetate C) [22].

It can be concluded that the monitor enables to study biofilm development and the hydraulic biofilm resistance.

3.2.2. Biofilm resistance with and without feed spacer

Feed spacers have been shown to play an important part in fouling [27–31]. In the present study, the effect of spacer presence on transmembrane hydraulic biofilm resistance was evaluated. The development of total resistance was studied using monitors with and without feed spacer and with and without nutrient dosage.

Regardless of feed spacer presence, the same initial transmembrane resistance and the same increase of total resistance was observed with nutrient supply (Fig. 9), at operating conditions (flux and crossflow) as applied in practice for spiral-wound NF and RO membrane elements. The monitor can be used to evaluate the effect of a feed spacer on hydraulic biofilm resistance.

3.2.3. FCP and transmembrane resistance

Biofilm formation can have a negative impact on NF and RO membrane performance by increasing the TMP and the FCP. Past and current monitors used for membrane biofouling research are suitable only to

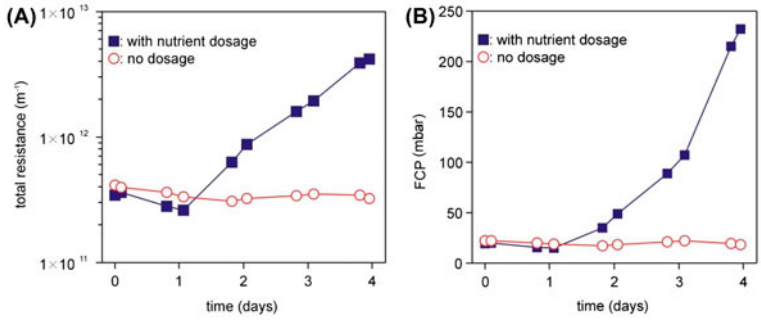

Fig. 10. Total resistance (A) and FCP (B) development over time at a flux of 20 L $m^{-2} h^{-1}$ and cross-flow velocity of 0.1 m s^{-1} with and without nutrient dosage (1 mg L^{-1} acetate (C)). The experiment was performed with feed spacer.

study either the TMP or the FCP. The increase of both, total transmembrane resistance and FCP could be determined using the newly developed tMBM. tMBMs containing a feed spacer were operated at a flux of $20\,L\,m^{-2}\,h^{-1}$ and a cross-flow velocity of $0.1\,m\,s^{-1}$ without and with nutrient dosage ($1\,mg\,L^{-1}$ acetate C).

With nutrient supply, both the transmembrane biofilm resistance and the FCP increased in time (Fig. 10).

The tMBM enables the assessment of biofilm formation effects on both the TMP and FCP. The presence of elevated nutrient concentrations in the feed water speeds up the biofilm formation, enabling to perform short-term biofouling studies.

4. Discussion

4.1. Evaluation of the tMBM

A transparent MBM is developed, enabling to study the hydraulic biofilm resistance and the direct impact of biofilm formation on the TMP and FCP. The tMBM is representative for spiral-wound membrane elements used in practice with regard to the materials used (membranes and spacers), spatial dimensions (height of feed and product spacer channels), hydraulics (FCP and flow distribution), and operational conditions (transmembrane flux and cross-flow velocity range: e.g. a flux of $20\,L\,m^{-2}\,h^{-1}$ and a cross-flow velocity of $0.1\,m\,s^{-1}$). Using the tMBM, fouling can be quantified and characterized by: (i) the increase of transmembrane resistance and FCP; (ii) *in situ*, real-time, and non-destructive observations; and (iii) analysis of membrane and spacer sampled from the tMBM. The scale of the tMBM makes handling easy, minimizes equipment and operation costs, and reduces chemical and water consumption. Compared to the description of an ideal monitor [16,32,33], the tMBM fulfills most requirements making it a well-suited tool for biofouling prediction and control research.

The microfiltration membrane (pore size 0.05 μm) used in the tMBM prevents salt concentration polarization and allows operation at low pressures, thus permitting accurate measurement of the intrinsic hydraulic biofilm resistance. The contribution of the membrane resistance to the total resistance is much smaller than the contribution of the hydraulic biofilm resistance (see Figs. 8–10) allowing more accurate measurements using standard pressure transducers. TMP and FCP measurements are sufficiently sensitive to allow the study of hydraulic biofilm resistance and development.

4.2. Application of the tMBM

Unique aspects of the tMBM, as illustrated in Section 3.1, are the possibilities to study and monitor the (i) hydraulic biofilm resistance, (ii) performance parameters FCP and TMP, and (iii) *in situ* spatially resolved observations of the biofilm thickness in the transparent MBM. The tMBM is suitable as a simulator for spiral-wound modules as previously discussed [19] and integrates well into the laboratory environment. Such biofouling studies can be performed with and without a feed spacer and the tMBM is adaptable to various spacer designs (thickness, geometry, and porosity) operated under varying conditions.

OCT was developed in 1991 by Huang et al. [34] as a tool for medical imaging. This relatively new optical method has the ability to non-destructively provide volumetric imaging of the biofilm with micron resolution [35–40]. Since 2006, the OCT has been used to study biofilm structures in water systems: degradation by a disinfectant [36], impact of flow conditions [37], mechanisms of *Escherichia coli* attachment on biofilms [40], and metazoan activity in relation to biofilm structure and flux in ultrafiltration membranes [38,39]. The tMBM is ideally suited for OCT studies of *in situ* biofilm development in membrane systems (Fig. 7). The OCT instrument axial resolution is less than 6 μm and the lateral resolution 8 μm. OCT images provide a quantitative high-resolution spatially-resolved means to characterize biofilm thickness, structural heterogeneity, growth, and detachment over large areas of membrane and spacer. Examples of studies could be the influence of operational parameters (flux and cross-flow velocity), spacer design (spacer geometry), and control strategies on biofilm development and removal. Such detailed biofilm studies may lead to novel and more effective strategies to control membrane biofouling.

Additional tools needed to complement current research techniques for gaining insight into membrane (bio)fouling characterization and control are: (i) a monitor with the length of a membrane module enabling direct visual observations of accumulated fouling and monitoring of all performance parameters (FCP, flux, and salt passage) during operation at pressures and conditions as applied in practice and (ii) a high pressure miniature monitor to unravel the relationship between concentration polarization, biofouling, and membrane performance. Since the low-pressure tMBM showed to be suitable for biofilm studies in membrane systems, a high-pressure version of tMBM is being developed.

4.3. Representativeness and validation of membrane biofouling monitors

In membrane conference papers and peer reviewed journals membrane biofouling monitors have been presented as suitable tools for biofouling control studies. In commercial brochures, membrane biofouling monitors have been advertised by their suppliers. In general, no data on monitor validation is included, while a critical evaluation of the representativeness of the monitor results for practice hardly exists. For a comprehensive understanding of the state of the art in biofouling control, it is essential to address and report monitor validation tests in peer-reviewed papers.

Many membrane biofouling monitor studies have been described, from which the laboratory conditions are not representative for conditions of pilot and full scale membrane installations. However, a biofouling control approach effective under non-representative laboratory conditions is most probably not predictive for industrial practice.

The results reported in this paper present a versatile tool for biofilm research and biofouling control that has been validated (Sections 3.1.1–3.1.4) under laboratory conditions representative for the application of spiral-wound membrane modules.

5. Conclusions

The results showed that the newly developed tMBM is representative for spiral-wound membrane elements with regard to spacer channel height and hydrodynamic behavior. The monitor is suitable for (i) measuring the feed channel pressure drop and TMP (ii) *in situ*, real-time and non-destructive (visual and optical) observations of accumulated material, and (iii) analysis of membrane and spacer from the tMBM. The monitor proved to be easy to handle.

The results presented in this paper led to the following conclusions for the tMBM:

(1) The tMBM can be used to quantify the intrinsic hydraulic biofilm resistance.
(2) The tMBM can be operated:
   (a) with and without feed spacer;
   (b) with and without permeate production;
   (c) at crossflow and flux conditions as applied in practice;
   (d) with several water types such as surface water, brackish water, and seawater.

Acknowledgments

This work was performed at Wetsus, Centre of Excellence for Sustainable Water Technology (www.wetsus.nl). Wetsus is funded by the Dutch Ministry of Economic Affairs, the European Union European Regional Development Fund, the Province of Fryslân, the city of Leeuwarden, and by the EZ-KOMPAS Program of the "Samenwerkingsverband Noord-Nederland." The authors like to thank the participants of the research theme "Biofouling" and Evides waterbedrijf for the fruitful discussions and their financial support. In addition, the authors would especially like to thank the students Malgorzata Nowak, Stanislaw Wojciechowski, Judita Laurinonyte, Nathalie Juranek, and Zhen Xiang for their great support with the experimental work in the laboratory. The photographs of the tMBM were taken by Christina Kappel and her work is herewith gratefully acknowledged.

Abbreviations

CFU	—	colony forming units
FCP	—	feed-channel pressure drop
J	—	flux
MBM	—	membrane biofouling monitor
MFS	—	membrane fouling simulator
NF	—	nanofiltration
OCT	—	optical coherence tomography
PES	—	polyethersulfone
PMMA	—	polymethylmethacrylate
R	—	resistance
RO	—	reverse osmosis
SEM	—	scanning electron microscopy
TCN	—	total cell number
tMBM	—	transparent membrane biofouling monitor
TMP	—	transmembrane pressure drop
TOC	—	total organic carbon
UF	—	ultrafiltration

Symbols

λ	—	friction coefficient (−)
η	—	dynamic viscosity (kg m^{-1} s^{-1})
ρ	—	specific liquid density (kg m^{-3})
A	—	membrane area (m^2)
d_h	—	hydraulic diameter (m)
J	—	permeate flux (m^3 m^{-2} s^{-1})
L	—	length (m)
P	—	pressure (bar)
R	—	resistance (m^{-1})
Re	—	Reynolds number (−)
t	—	time (h)
V	—	volume (L)
v	—	linear velocity of water (m s^{-1})

References

[1] M.A. Shannon, P.W. Bohn, M. Elimelech, J.G. Georgiadis, B.J. Mariñas, A.M. Mayes, Science and technology for water purification in the coming decades, Nature 452 (2008) 301–310.

[2] J.S. Baker, L.Y. Dudley, Biofouling in membrane systems—A review, Desalination 118 (1998) 81–89.

[3] H.F. Ridgway, H.C. Flemming, Biofouling of membranes, in: J. Mallevialle, P.E. Odendaal, M.R. Wiesner (Ed.), Water treatment membrane processes, McGraw-Hill, New York, NY, 1996, pp. 629–640.

[4] H.F. Ridgway, A. Kelly, C. Justice, B.H. Olson, Microbial fouling of reverse-osmosis membranes used in advanced wastewater treatment technology: Chemical, bacteriological, and ultrastructural analyses, Appl. Environ. Microbiol. 45 (1983) 1066–1084.

[5] R.P. Schneider, L.M. Ferreira, P. Binder, E.M. Bejarano, K.P. Góes, E. Slongo, C.R. Machado, G.M.Z. Rosa, Dynamics of organic carbon and of bacterial populations in a conventional pretreatment train of a reverse osmosis unit experiencing severe biofouling, J. Membr. Sci. 266 (2005) 18–29.

[6] K. Tasaka, T. Katsura, H. Iwahori, Y. Kamiyama, Analysis of RO elements operated at more than 80 plants in Japan, Desalination 96 (1994) 259–272.

[7] J.S. Vrouwenvelder, S.A. Manolarakis, J.P. van der Hoek, J.A.M. van Paassen, W.G.J. van der Meer, J.M.C. van Agtmaal, H.D.M. Prummel, J.C. Kruithof, M.C.M. van Loosdrecht, Quantitative biofouling diagnosis in full scale nanofiltration and reverse osmosis installations, Water Res. 42 (2008) 4856–4868.

[8] H. Huiting, J.W.N.M. Kappelhof, T.G.J. Bosklopper, Operation of NF/RO plants: From reactive to proactive, Desalination 139 (2001) 183–189.

[9] M.M. Nederlof, J.C. Kruithof, J.S. Taylor, D. van der Kooij, J.C. Schippers, Comparison of NF/RO membrane performance in integrated membrane systems, Desalination 131 (2000) 257–269.

[10] P.A. Araújo, J.C. Kruithof, M.C.M. Van Van Loosdrecht, J.S. Vrouwenvelder, The potential of standard and modified feed spacers for biofouling control, J. Membr. Sci. 403–404 (2012) 58–70.

[11] S.A. Creber, J.S. Vrouwenvelder, M.C.M. van Loosdrecht, M.L. Johns, Chemical cleaning of biofouling in reverse osmosis membranes evaluated using magnetic resonance imaging, J. Membr. Sci. 362 (2010) 202–210.

[12] D.J. Miller, P.A. Araújo, P.B. Correia, M.M. Ramsey, J.C. Kruithof, M.C.M. van Loosdrecht, B.D. Freeman, D.R. Paul, M. Whiteley, J.S. Vrouwenvelder, Short-term adhesion and long-term biofouling testing of polydopamine and poly(ethylene glycol) surface modifications of membranes and feed spacers for biofouling control, Water Res. 46 (2012) 3737–3753.

[13] E.I. Prest, M. Staal, M. Kühl, M.C.M. van Loosdrecht, J.S. Vrouwenvelder, Quantitative measurement and visualization of biofilm O2 consumption rates in membrane filtration systems. J. Membr. Sci. 392–393 (2012) 66–75.

[14] J.S. Vrouwenvelder, J. Buiter, M. Riviere, W.G.J. van der Meer, M.C.M. van Loosdrecht, J.C. Kruithof, Impact of flow regime on pressure drop increase and biomass accumulation and morphology in membrane systems, Water Res. 44 (2010) 689–702.

[15] J.S. Vrouwenvelder, C. Hinrichs, W.G.J. Van der Meer, M.C.M. Van Loosdrecht, J.C. Kruithof, Pressure drop increase by biofilm accumulation in spiral wound RO and NF membrane systems: Role of substrate concentration, flow velocity, substrate load and flow direction, Biofouling 25 (2009) 543–555.

[16] J.S. Vrouwenvelder, S.M. Bakker, M. Cauchard, R. Le Grand, M. Apacandié, M. Idrissi, S. Lagrave, L.P. Wessels, J.A.M. van Paassen, J.C. Kruithof, M.C.M. van Loosdrecht, The membrane fouling simulator: A suitable tool for prediction and characterisation of membrane fouling, Water Sci. Technol. 55 (2007) 197–205.

[17] J.S. Vrouwenvelder, S.M. Bakker, L.P. Wessels, J.A.M. van Paassen, The membrane fouling simulator as a new tool for biofouling control of spiral-wound membranes, Desalination 204 (2007) 170–174.

[18] J.S. Vrouwenvelder, J.A.M. Van Paassen, L.P. Wessels, A.F. Van Dam, S.M. Bakker, The membrane fouling simulator: A practical tool for fouling prediction and control, J. Membr. Sci. 281 (2006) 316–324.

[19] G. Schock, A. Miquel, Mass transfer and pressure loss in spiral wound modules, Desalination 64 (1987) 339–352.

[20] W.G.J. van der Meer, Mathematical modeling of NF and RO membrane filtration plants and modules in PhD thesis, 2003.

[21] J.S. Vrouwenvelder, M.C.M. Van Loosdrecht, J.C. Kruithof, A novel scenario for biofouling control of spiral wound membrane systems, Water Res. 45 (2011) 3890–3898.

[22] C. Dreszer, J.S. Vrouwenvelder, A.H. Paulitsch-Fuchs, A. Zwijnenburg, J.C. Kruithof, H.C. Flemming, Hydraulic resistance of biofilms, J. Membr. Sci. 429 (2013) 436–447.

[23] D.J. Reasoner, E.E. Geldreich, A new medium for the enumeration and subculture of bacteria from potable water, Appl. Environ. Microbiol. 49 (1985) 1–7.

[24] K. Lautenschlager, C. Hwang, W.T. Liu, N. Boon, O. Köster, H. Vrouwenvelder, T. Egli, F.A. Hammes, A microbiology-based multi-parametric approach towards assessing biological stability in drinking water distribution networks, Water Res. 47 (2013) 3015–3025.

[25] F. Hammes, M. Berney, Y. Wang, M. Vital, O. Köster, T. Egli, Flow-cytometric total bacterial cell counts as a descriptive microbiological parameter for drinking water treatment processes, Water Res. 42 (2008) 269–277.

[26] D. Van Gauwbergen, J. Baeyens, Macroscopic fluid flow conditions in spiral-wound membrane elements, Desalination 110 (1997) 287–299.

[27] J. Baker, T. Stephenson, S. Dard, P. Côté, Characterisation of fouling of nanofiltration membranes used to treat surface waters, Environ. Technol. 16 (1995) 977–985.

[28] S.R. Suwarno, X. Chen, T.H. Chong, V.L. Puspitasari, D. McDougald, Y. Cohen, S.A. Rice, A.G. Fane, The impact of flux and spacers on biofilm development on reverse osmosis membranes, J. Membr. Sci. 405–406 (2012) 219–232.

[29] T. Tran, B. Bolto, S. Gray, M. Hoang, E. Ostarcevic, An autopsy study of a fouled reverse osmosis membrane element used in a brackish water treatment plant, Water Res. 41 (2007) 3915–3923.

[30] J.A.M. van Paassen, J.C. Kruithof, S.M. Bakker, F.S. Kegel, Integrated multi-objective membrane systems for surface water treatment: Pre-treatment of nanofiltration by riverbank filtration and conventional ground water treatment, Desalination 118 (1998) 239–248.
[31] J.S. Vrouwenvelder, D.A. Graf von der Schulenburg, J.C. Kruithof, M.L. Johns, M.C.M. van Loosdrecht, Biofouling of spiral-wound nanofiltration and reverse osmosis membranes: A feed spacer problem, Water Res. 43 (2009) 583–594.
[32] H.C. Flemming, Role and levels of real-time monitoring for successful anti-fouling strategies—an overview, Water Sci. Technol. 47 (2003) 1–8.
[33] H.-C. Flemming, A. Tamachkiarowa, J. Klahre, J. Schmitt, Monitoring of fouling and biofouling in technical systems, Water Sci. Technol. 38 (1998) 291–298.
[34] D. Huang, E.A. Swanson, C.P. Lin, J.S. Schuman, W.G. Stinson, W. Chang, M.R. Hee, T. Flotte, K. Gregory, C.A. Puliafito, J.G. Fujimoto, Optical coherence tomography, Science 254 (1991) 1178–1181.
[35] C. Xi, D. Marks, S. Schlachter, W. Luo, S.A. Boppart, High-resolution three-dimensional imaging of biofilm development using optical coherence tomography, J. Biomed. Opt. 11 (2006) 034001–034001.
[36] C. Haisch, R. Niessner, Visualisation of transient processes in biofilms by optical coherence tomography, Water Res. 41 (2007) 2467–2472.
[37] M. Wagner, D. Taherzadeh, C. Haisch, H. Horn, Investigation of the mesoscale structure and volumetric features of biofilms using optical coherence tomography, Biotechnol. Bioeng. 107 (2010) 844–853.
[38] N. Derlon, M. Peter-Varbanets, A. Scheidegger, W. Pronk, E. Morgenroth, Predation influences the structure of biofilm developed on ultrafiltration membranes, Water Res. 46 (2012) 3323–3333.
[39] N. Derlon, N. Koch, B. Eugster, T. Posch, J. Pernthaler, W. Pronk, E. Morgenroth, Activity of metazoa governs biofilm structure formation and enhances permeate flux during Gravity-Driven Membrane (GDM) filtration, Water Res. 47 (2013) 2085–2095.
[40] D. Janjaroen, F. Ling, G. Monroy, N. Derlon, E. Mogenroth, S.A. Boppart, W.-T. Liu, T.H. Nguyen, Roles of ionic strength and biofilm roughness on adhesion kinetics of *Escherichia coli* onto groundwater biofilm grown on PVC surfaces, Water Res. 47 (2013) 2531–2542.